Project no. TIP5-CT-2006-031415O

INNOTRACK

Integrated Project (IP)

Thematic Priority 6: Sustainable Development, Global Change and Ecosystems

D4.2.3
Improved model for loading and subsequent deterioration of insulated joints

Due date of deliverable: 2009-02-28

Actual submission date: 2009-02-28

Start date of project: 1 September 2006 Duration: 36 months

Organisation name of lead contractor for this deliverable: Chalmers

Revision: Final

Project co-funded by the European Commission within the Sixth Framework Programme (2002-2006)		
Dissemination Level		
PU	Public	PU
PP	Restricted to other programme participants (including the Commission Services)	
RE	Restricted to a group specified by the consortium (including the Commission Services)	
CO	Confidential, only for members of the consortium (including the Commission Services)	

Table of Contents

1. Executive Summary

Numerical simulations have been carried out to assess the influence of key parameters on the deterioration of insulated joints. The measures of fatigue damage were adopted; one low-cycle fatigue based and one ratcheting based. Both of these models are based on the stress–strain evolution, which consequently needs to be accurately modelled. This calls for a constitutive model that can deal with plasticity under general multi-axial loading. In the current study the material parameters in the constitutive model have been calibrated to reflect the characteristics of the rail steel grade 900A.

The simulations verify previous findings that the insulating layer does not carry any significant load. Consequently severe strains occur at the rail head edge. The ratcheting based fatigue criterion was found to be the most suitable for the current study and the accumulated plastic strain after four load passages, $\varepsilon_{\mathrm{eff}}$, was adopted to quantify the ratcheting. The numerical simulations showed that increasing the insulating gap from 4 mm to 6 mm gives roughly the same effect as an increase of the vertical load from 150 kN to 200 kN, which is an increase in $\varepsilon_{\mathrm{eff}}$ of about 10%. In addition, a very detrimental effect of traction and braking was found: Increasing the longitudinal load from 0 kN up to 45 kN caused an increase in $\varepsilon_{\mathrm{eff}}$ magnitudes with up to 95%.

The predictions of plastic deformation and rolling contact fatigue have been performed. A fixed traction coefficient was presumed giving a wear pattern that is a linear function of pressure, which is in turn proportional to the cube-root of the applied normal force. The highest wear is predicted immediately after the insulated joint, with additional high-wear spots appearing a few metres later as the wheel bounces down and settles.

In addition to numerical simulations four operational joints have been monitored in field to follow the degradation. It was found that material damage is induced very fast. In accordance to numerical simulations the rail ends closest to a nearby station showed the largest degree of damage. This damage had a wear-like appearance. After 8 months it was found that also “cavity-like” damages had formed in the vicinity of the insulating joint.

2. Introduction

The overall objectives of Work Package (WP) 4.2 are (see the INNOTRACK Description of Work):

- To evaluate tolerances and limits for rails and joint degradation in terms of allowable magnitudes of wear, corrugation, geometrical deviations, etc under different operational conditions.
- To establish minimum action rules for the occurrence of material defects under different operational conditions and rail/joint degradation

This deliverable is a step towards these objectives. Note that the title of the deliverable has been changed from the original title "Improved model for deterioration due to point-like rail defects". The reason is that the other study of point-like defect that was planned to be included in this study, namely singular squats, has been moved to D4.2.4.

To further detail the contributions of WP 4.2 and its interaction to other Sub-Projects (SP) and WPs, it was clarified at the WP 4.2 meeting 15th of February 2007 that the focus in WP4.2 is mainly on vertical train–track interaction and related deterioration. In addition longitudinal forces due to braking/traction will be included when suitable. Analysis of lateral train–track interaction and subsequent deterioration calls for vehicle models that are largely lacking or are not available for use in INNOTRACK. This topic is therefore left for the low- and medium-resolution modelling of SP1. This includes e.g. prediction of the formation of head checks. In addition to SP1, lateral train–track dynamics and subsequent deterioration will also to some extent be studied in SP3 and WP4.3.

Within these frames, the work within WP4.2 includes the collection of input and validation data and actual numerical simulation and resulting quantifications of increased operational loads and deteriorations.

The current deliverable report focuses on "singular" irregularities. The definition of a "singular" irregularity is of course prone to be rough. After discussions in the work package it was concluded that the border case of squats (which may occur in clusters or single) are dealt with in D4.2.4. In addition the case of switches and crossings, which may also be seen as "singular" irregularities are dealt with in work package WP3.1: Switches & Crossings. This left the study of insulated joints for the current deliverable report. The report was renamed to match this more narrow focus.

In WP4.2 there are three aspects regarding the loading and deterioration of insulated joints that are studied:

- The loading on insulated joints by passing wheels and how this loading is influenced by vehicle speed and vertical misalignment of the railhead at the insulating layer. This topic has been studied and reported in deliverable report D4.2.1.
- The influence on passing vehicles by the load imposed by negotiating a singular irregularity. This issue has also been studied and reported in D4.2.1.
- The material deterioration caused by the imposed loading. This issue will be reported in the current deliverable as detailed below.

The conclusions from all of these studies will be compiled in deliverable D4.2.6.

Large parts of the work presented in this deliverable report is also presented in the Licentiate Thesis (Johan Sandström, 2008) that has been presented at a public seminar featuring Anders Frick of the Swedish National Rail Administration, Banverket as discussion leader. In addition the paper in appendix I has been peer reviewed and accepted for publication in IMechE Journal of Rail and Rapid Transit. We consider this as important parts in the quality assurance, dissemination and acceptability for future implementation of the research outcome presented in this deliverable.

3. Deterioration of insulated joints

3.1 Background

Insulated joints are common in railroads. Their function is to electrically insulate two sections of a track from each other. The sectioning is utilized for signalling purposes: When a train operates on a track section its wheelset will short-circuit the rails. If it can be identified which track section that is short-circuited the position of the train is known.

Insulating joints can be designed in different ways. A normal configuration is that the rail is cut transversally and an insulated polymer layer is placed (glued) in the gap between the rail ends. The joint is assembled using two beams (fishplates) that are bolted to each side of the rail, see Figure 1. The joint is often prefabricated and the joint section assembled in the track by welding.

Figure 1 *A newly installed insulated joint on The West Coast Line in Sweden*

Insulating joints are weak points of the rail that frequently cause problems. This can be attributed to the mechanical characteristics of an insulated joint. The joint imposes a sudden variation in track stiffness due to the change in bending and shear stiffness of the rail and the added weight of the fishplates. Further wheel–rail impact loads are often generated at insulated joints because of a local rail surface irregularity caused by misalignment and plastic deformations of the rail ends, see (Kabo et al., 2006). In addition, the insulating layer is very flexible in comparison to the rail. In practice the insulating gap can therefore be considered as a free end of the rail. This results in a severe stress concentration at the insulating layer.

The study on insulating joints presented here focuses on the wheel–rail contact and its consequences on subsequent deterioration. It draws on initial studies at CHARMEC (Elena Kabo, 2004; Kabo et al., 2006; Johan Sandström et al., 2006). In addition wear predictions have been carried out to investigate how an insulating joint influences the wear pattern. In addition there are also studies in the literature that relate to contact stresses in the wheel–rail interface at joint negotiation (Yung-Chuan Chen and Li-Wen Chen, 2006; Yung-Chuan Chen and Kuang, 2002) and to interfacial stresses between the rail and the insulating material (Himebaugha et al., 2008; Plaut et al., 2007).

A fundamental question in the study of mechanical deterioration of insulated joints is whether an increased joint gap will alleviate or aggravate the problem with deteriorated insulated joints. That the answer is not straightforward is indicated by the fact that joint gaps currently adopted vary. In order to answer this question more in-depth knowledge on the consequences of altered insulating gaps is needed. To this end, a detailed study of the deterioration of the rail material in the joint close to the insulating layer is performed. There the material accumulates plastic deformations, which leads to material failure causing chips of metal to break off. This may result in the formation of an electrically conductive bridge over the insulating layer, causing malfunction of the signalling system. In Figure 2 a deteriorated insulated joint is shown. Other failure modes for insulated joints include run-down of the joints resulting in a dipped joint that will cause high vertical load magnitudes and subsequent secondary damages (see INNOTRACK deliverable D4.2.1). Also formation of corrugation and squats are rather common in the vicinity of an insulated joint due to the non-continuous track stiffness at the joint.

The paper presented in Appendix I takes the aim at quantifying the damage to make way for a comparison between different operational scenarios in terms of loading and joint geometry.

Figure 2 *A severely deteriorated insulated joint.*

3.2 Field studies

Field tests were initiated on Västkustbanan (the West Coast Line in Sweden) near the city of Falkenberg in the summer of 2008. Newly installed insulated joints on a double track are being monitored. The joints are located about 300 meters from Falkenberg station. The maximum allowed speed on the line is 200 km/h. The traffic is mixed with a highest axle load of 22.5 tonnes and distributed load 6.5 tonnes/meter (the track is designed for 25 tonnes). Based on number of axles passing a nearby hot wheel detector in Morup, the operational load was estimated to be in the order of 5 to 6 MGT/track/year.

The mix of traffic is shown in Figure 3. In evaluating the operational load, it was assumed that freight trains have a mean axle weight of 14.25 tonnes (50 % empty). Passenger train is assumed to have a mean axle weight of 13.85 tonnes.

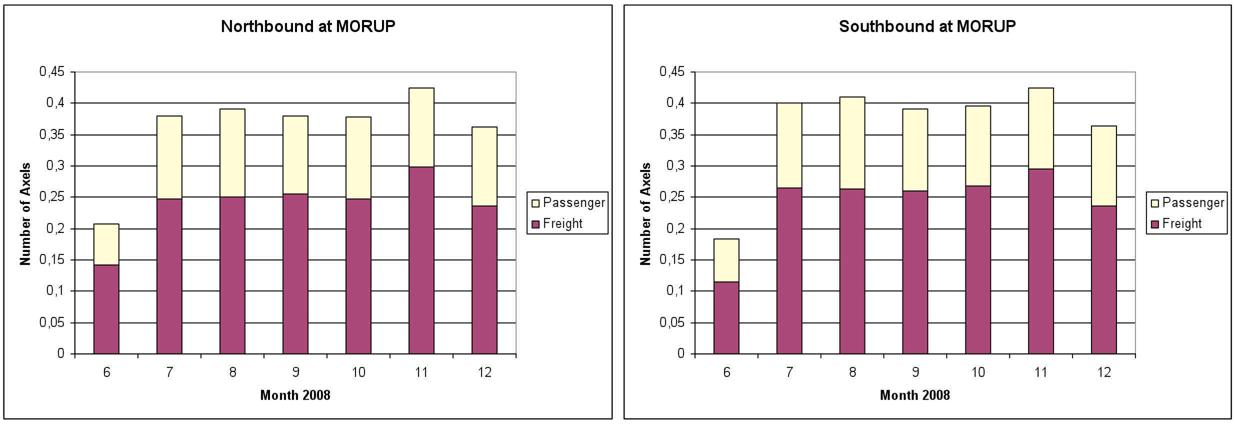

Figure 3 *Estimated traffic June to December 2008 at the monitored insulated joints. Picture courtesy Arne Nissen, Banverket. In the period June 15th – December 31st 2008 the total MGT is 2.5 northbound and 2.6 southbound.*

Field measurements have been carried out at three occasions 2008-06-11 (the week before the start of operational traffic, but after grinding), 2008-08-20 and 2009-02-20. At all occasions the inclination of the joint was estimated visually. The measurement showed no run down of the joint. Further the damage of the joint was documented and the rail hardness in the vicinity of the joint measured. The results from hardness measurements are at this moment still inconclusive. The measuring campaign will continue.

The conditions of the joints at the measurements 2008-08-20 are shown in Figure 4. It is seen that on all four joints the rail end towards the station showed most sign of damage. This supports the simulation results regarding the influence of the direction of the longitudinal force since these are the rail ends that get compressed by the longitudinal wheel–rail interfacial force from traction (when accelerating from the station) and braking (when stopping at the station). It could also indicate that the vertical impact, which is highest on the running-on rail end (Kabo et al., 2006) is not the dominating cause of damage, at least not when relatively high longitudinal wheel–rail forces exist.

The subsequent measurements in 2009-02-20 confirmed this pattern, but also revealed a new damage mode: On two of the joints (the joints towards the field sides) of a more “cavity-like” damage was found on the opposite side of the joint, as seen in the lowest photo of Figure 5.

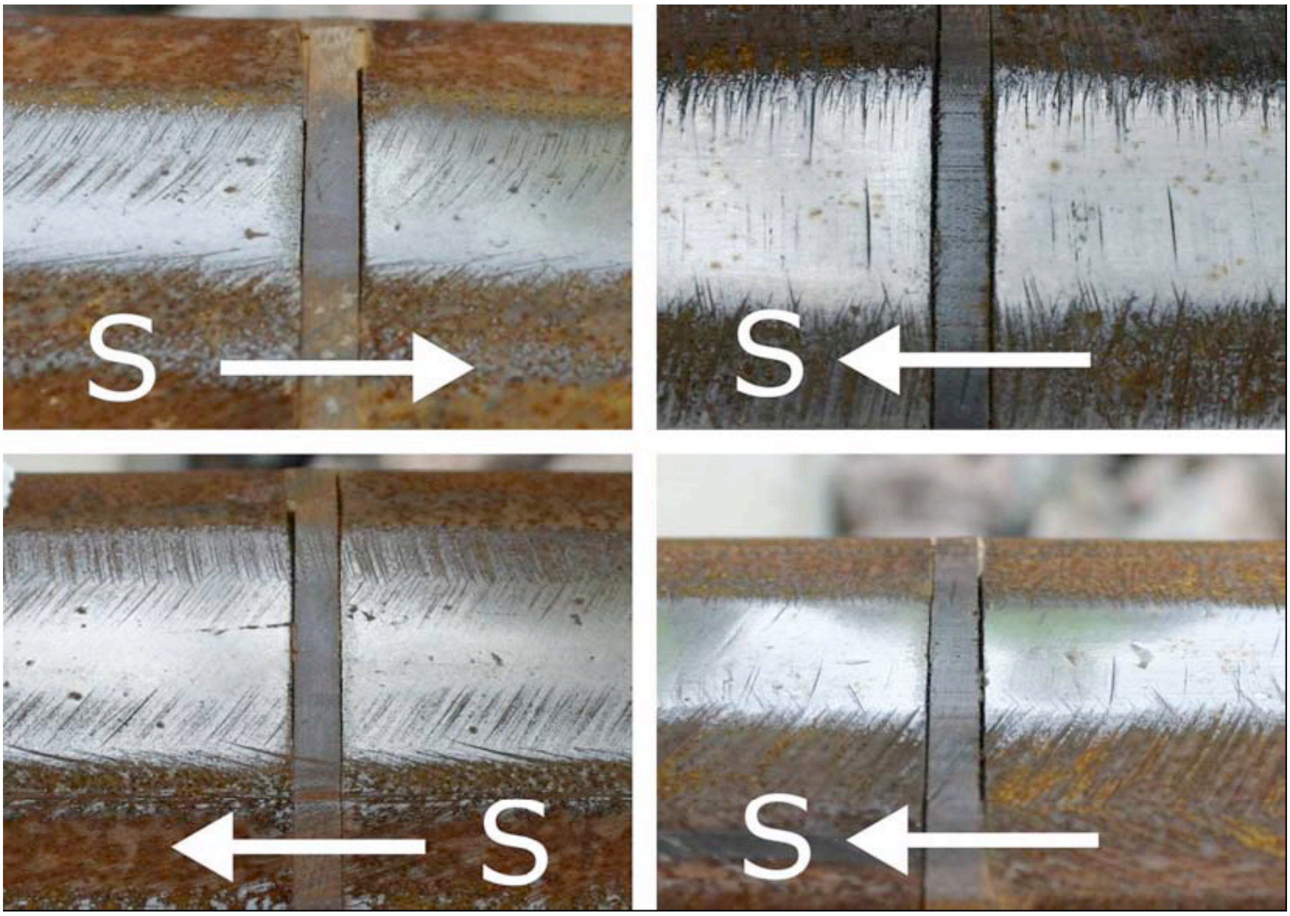

Figure 4 *The four observed insulating joints in 2008-08-20 (roughly two months after operations started). The sides towards the station are marked with an S and the main travelling direction of the passing trains is marked with an arrow. Note also the detachment of the insulating layer.*

Figure 5 *Damage evolution of an insulated joint. From top to bottom: 2008-06-11 (the week before the start of operational traffic, but after grinding), 2008-08-20 and 2009-02-20.*

3.3 Numerical modelling of plastic deformation and rolling contact fatigue of insulated joints

The damage mechanism is presumed to be low cycle fatigue (including ratcheting). To quantify the damage an elastic-plastic analysis is needed to derive the evolution of strains and stresses in the rail joint during the negotiation of a wheel. Two different fatigue criteria are employed. The first criterion is based on the ratcheting mechanism, i.e. the continuous accumulation of plastic deformation. As a measure of the multiaxial strain, an effective strain is evaluated

$$\varepsilon_{\text{eff}} = \frac{\sqrt{2}}{3}\sqrt{\left(\varepsilon_{xx}-\varepsilon_{yy}\right)^2+\left(\varepsilon_{yy}-\varepsilon_{zz}\right)^2+\left(\varepsilon_{zz}-\varepsilon_{xx}\right)^2+6\left(\varepsilon_{xy}^2+\varepsilon_{yx}^2+\varepsilon_{zx}^2\right)} \tag{1}$$

The effective strain after four completed load cycles (wheel rollovers) is taken as the comparative damage measure.

The second criterion employed is a multiaxial low-cycle fatigue criterion proposed for rolling contact fatigue (Jiang & Sehitoglu, 1999). This criterion quantifies the fatigue damage by a fatigue parameter

$$FP = \Delta\varepsilon\langle\sigma_{\max}\rangle + c_{\mathrm{j}}\Delta\gamma\Delta\tau \tag{2}$$

The criterion is evaluated for a critical material plane where $\Delta\varepsilon$ is the range of the normal strain acting on the plane, $\langle\sigma_{\max}\rangle = \max\{\sigma_{\max},0\}$ is the largest normal stress on the plane. Further c_{j} is a material parameter, $\Delta\gamma$ the range of the engineering shear strain and $\Delta\tau$ the range of the shear stress. In the literature there are a number of other multiaxial low-cycle fatigue criteria, which could have been employed, see (Socie & Marquis, 2000).

Both estimations of fatigue damage are based on the stress–strain evolution, which consequently needs to be accurately modelled. This calls for a constitutive model that can deal with plasticity under general multi-axial loading. Such a model with suitable properties was developed in the thesis (Johansson, 2006). The application in (Johansson, 2006) is towards rail steel in switches, which regarding load magnitudes and contact patch sizes similar to the conditions at insulated joints. In the current study the material parameters in the constitutive model have been calibrated to reflect the characteristics of the rail steel grade 900A (R260) (Johansson et al., 2006).

For the simulation of the quasi-static rolling of the wheel over the joint, a non-linear finite element (FE) analysis is used. The commercial FE–code Abaqus is used due to its ability to include custom material models and its capability to handle contact problems. The geometrical model consists of a wheel section rolling over a part of the joint. A reference case with a vertical (quasi-static) wheel load of 150 kN and an insulating gap width of 4 mm was employed.

Two significant difficulties in the simulations are to obtain numerical convergence and to limit simulation times. There are a number of reasons for these problems. The use of contact algorithms together with custom elastic–plastic material leads to convergence difficulties and requirements on very short time steps. Also a dense finite element mesh is needed to obtain a reasonable reliability of results close to the wheel–rail contact. Further, the computational domain employed in the simulations needs to be rather large in the longitudinal rail direction to be able to accommodate the distance traversed by the wheel. Therefore the number of elements becomes substantial. Another problem encountered is to establish wheel–rail contact at the start of the second (and later) wheel passage(s). This is likely due to the gap developed between initial positions of the wheel and rail due to plastic deformations of the rail. The built in feature of damped viscous contact in Abaqus v6.5 does not solve this issue satisfactorily. Instead a spring is introduced to restrain the wheel in the initial phase of the normal loading stage, as visualized in Figure 6a.

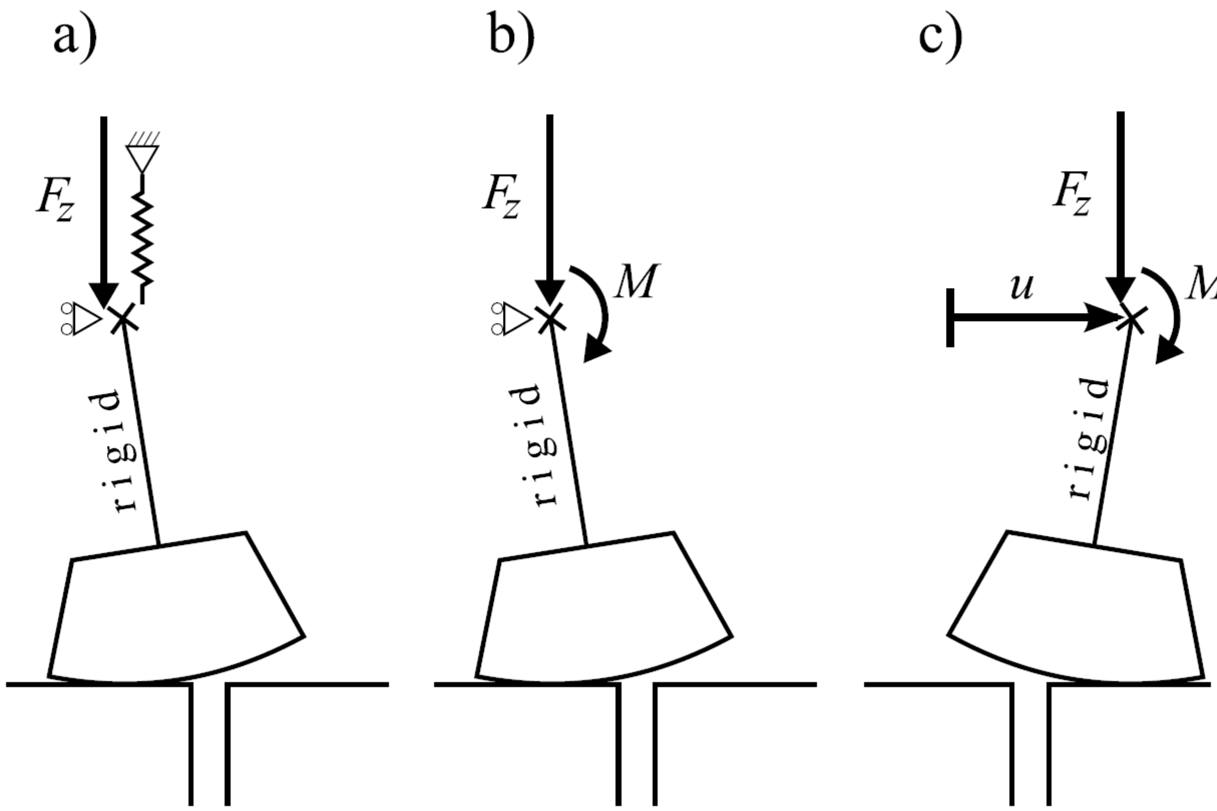

Figure 6 *Loading (and boundary conditions) of the rolling wheel in the simulations.*

From the FE-simulation results fatigue impact is, as mentioned above, quantified by the fatigue parameter FP and by the effective strain. An additional measure employed was the depth of the plastic zone in the rail. The simulations indicate that FP is an inconclusive measure with difficulty to capture physically motivated trends — FP can even decrease with increased load. The effective strain seems to be a more conclusive measure and is therefore adopted as the main measure of the fatigue impact. A parametric variation shows a high influence of the longitudinal force (traction or braking) on the fatigue impact. For the reference case (vertical wheel load of 150 kN and insulating gap width of 4 mm) tractive forces of 0 kN, 30 kN and 45 kN induce residual effective stresses at the rail edge of 1.58 %, 1.74 % and 3.08 % respectively after four wheel passages.

An important and perhaps unexpected finding from the simulations is that the highest deterioration of the rail is at the rail end where the longitudinal wheel–rail interfacial force compresses the rail (i.e. in the leading end in braking and the trailing end in traction). The explanation to this behaviour is that the surface traction on the rail "lifts" the compressed rail end and forces the stretched rail end down. The increased fatigue impact is then a consequence of the increased contact pressure on the "lifted" rail end.

3.3.1 Brief summary of some key results

Below are definition of coordinate system, points of result evaluation, and a summary of selected parametric results. Details are given in Appendix I.

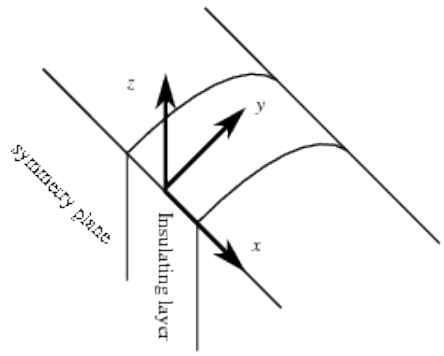

Figure 7 *Employed coordinate system.*

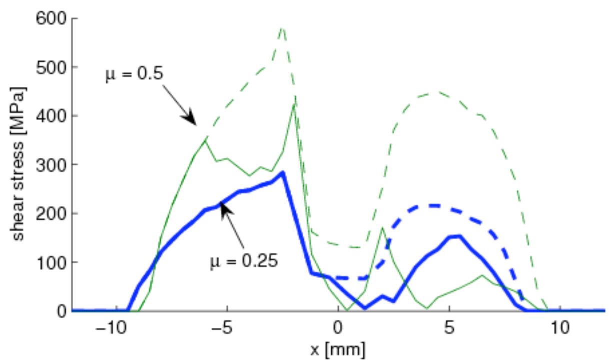

Figure 8 *Contact pressure distribution along the x-axis for y = 0 and along the y-direction for x = − 2.5 when the wheel is centered on the insulating joint. The solid line denotes the first wheel passage and the broken line the fourth passage. Fz = 150 kN, f = 0.2, μ = 0.25 and δ = 4 mm.*

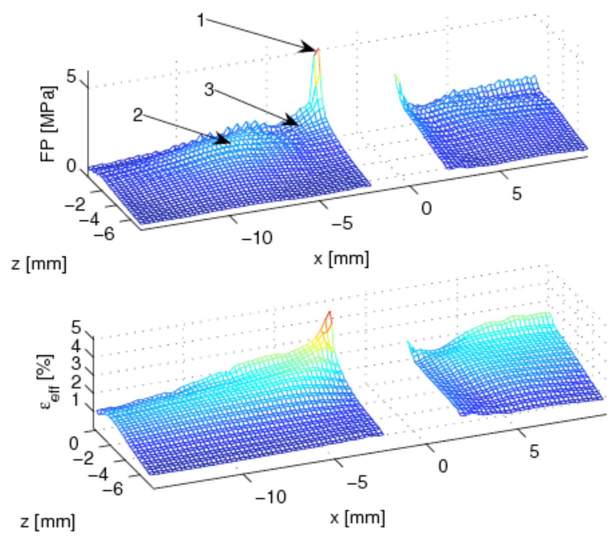

Figure 9 *Effective strain magnitudes in the symmetry plane corresponding to a vertical load F_z = 150 kN, traction coefficient f = 0.2, maximum coefficient of friction μ = 0.25 and insulation joint gap δ = 4 mm.. 1, 2 and 3 indicates where FP according to equation (2) is evaluated. The effective strain, ε_{eff} according to equation (1) is evaluated at position 3.*

μ	FP_1[MPa]	FP_2[MPa]	FP_3[MPa]	ε_{eff}[%]
0.25	4.35	1.06	1.0	1.76 / 2.44
0.5	5.36	1.10	1.02	2.01 / 2.71

The above table shows the influence of maximum coefficient of friction. The two magnitudes of ε_{eff} in the tables denote the residual strain and the maximum strain during loading, respectively.

δ	F_z[kN]	FP_1[MPa]	FP_2[MPa]	FP_3[MPa]	ε_{eff}[%]
4	150	5.12	1.65	1.22	1.74 / 2.47
	200	5.66	1.37	1.80	1.84 / 2.63
6	150	5.29	1.69	1.27	1.9 / 2.67
	200	6.67	1.95	1.51	2.06 / 2.92
8	150	5.34	1.91	1.38	2.05 / 2.84
	200	5.74	1.97	1.46	2.11 / 2.96

Influence of joint gap, δ, and vertical load magnitude, F_z. The applied lateral loading is defined by $\mu = 0.25$ and $f = 0.2$.

F_x[kN]	f	FP_1[MPa]	FP_2[MPa]	FP_3[MPa]	ε_{eff}[%]
-45	-0.3	7.66	1.19	1.31	2.39 / 3.23
-30	-0.2	4.35	1.06	1.0	1.76 / 2.44
0	0.0	3.51	1.19	1.02	1.58 / 2.19
30	0.2	5.12	1.65	1.22	1.74 / 2.47
45	0.3	11.3	2.69	2.04	3.08 / 4.1

Influence of lateral loading, F_x. The applied vertical loading is $F_z = 150$ kN and the insulation gap $\delta = 4$ mm. The maximum coefficient of friction is set to $\mu = 0.25$ for $|f| \leq 0.2$ and $\mu = 0.5$ for $|f| > 0.2$.

3.3.2 Possible improvements in numerical simulations

The identification of ratcheting as a dominating damage mechanism opens up for the use of a simplified constitutive model as compared to the paper in Appendix I. To model the stress–strain response as in Figure 10a several so-called back-stresses need to be employed. This makes the numerical simulations more cumbersome since the constitutive model gets more complex and the introduction of additional variables causes the solution at a time increment to be more expensive. The simulation will therefore be much more sensitive to the chosen time increments. In addition the solution is sensitive to previous time steps in that the solution can diverge also for very small time increments due to a previous time increment being to large. The capability of FE-solvers to automatically decrease time increment lengths is then useless. As a consequence very small time increments may be required for the whole load step, which leads to excessive computations. However, as it is established that ratcheting is of primary interest, future simulations could feature a more stable constitutive model with fewer back-stresses. This has the drawback of not capturing the full strain variation. However to quantify the ratcheting there is only a need to correctly capture the stress variation and the accumulated strain (ratcheting) as in Figure 10b.

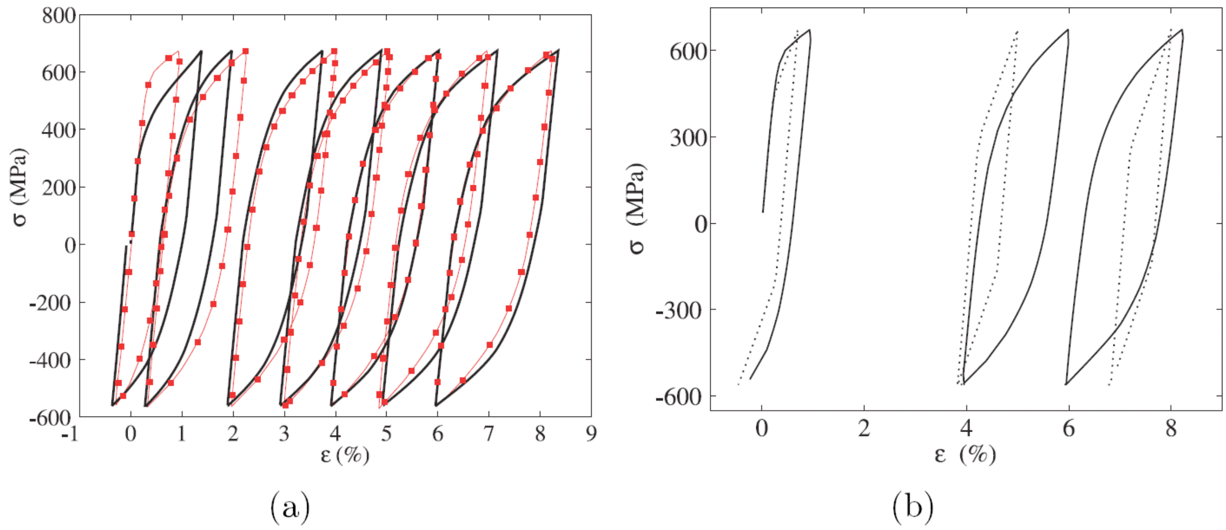

Figure 10 *Stress–strain response from experiments (square-dotted) and from the calibrated constitutive model (solid line). Figure (a) shows cycle 1, 25, 225, 425, 625, 825 and 1023 for a model with four backstresses and (b) shows cycle 1, 625 and 1023 for a model with only one backstress. Provided by G. Johansson and M. Ekh, Chalmers University of Technology*

Another topic for future studies is to employ material parameters for head-hardened rail steel as is commonly used in insulated joints. Dynamic loading at the joint could also be roughly accounted for by modifying the vertical wheel load during the wheel passage over the joint according to a dynamic simulation, (Kabo et al., 2006). This will introduce the train velocity as an additional parameter. The variation of contact force magnitudes due to increased speed and rail dip for an operational case is given in INNOTRACK Deliverable D4.2.1. In the current study the joint is presumed to be aligned (i.e. the joint dip is zero).

Although the computational times are rather large, improved numerical methods and faster computers would make the presented simulations cheaper and more usable in industry. Then other wheel–rail setups and insulated joint designs could be evaluated. A design modification in operation is where the insulated layer is inclined (non-perpendicular to the longitudinal rail direction) as exists in operation. Other improvements of the analysis could be to include anisotropic material properties in the constitutive model, as described in (Johansson & Ekh, 2006). Another feature developed for the constitutive model in (Johansson et al., 2005) is a capability that allows for several roll-overs to be simulated in one computed roll over (Johansson & Ekh, 2007). Error control would be used to control the number of roll-overs that can be simulated at once. This would allow simulating the actual long-term deformation, as compared to the so far simulation of fatigue and damage after just four load passages. Also of interest could be to include strain rate dependence in the constitutive model.

3.4 Wear prediction

A wear rate equation is developed in INNOTRACK Deliverable D4.2.5 for an elliptic wheel-rail contact patch with a fixed elliptic ratio (longitudinal semi-contact width over transverse semi-contact width) of 1.32, derived for wheel-rail contact on top of the rail head (i.e., appropriate for straight track, not curves). The average wear rate over the first 100000 wheel passes is given by:

$$\overline{w} = 0.2\frac{t_c}{\mu}\left(3 - \frac{t_c}{\mu}\right)^2 \left(2.3226p - 0.6761\right)$$

where p is peak pressure [in GPa], t_c is the traction coefficient, and w is average wear rate [in nm/cycle]; friction coefficient is fixed as μ=0.45, suitable for dry conditions. The asymptotic wear rate (i.e., the 'steady state' wear rate, usually achieved by 100000 cycles) is given by:

$$\underset{\rightarrow}{w} = 0.2\frac{t_c}{\mu}\left(3 - \frac{t_c}{\mu}\right)^2 \left(2.5513p - 0.5579\right)$$

To calculate profile area loss, the wear rate should be multiplied by the width of the contact.

These equations can be used to predict rail surface change through wear caused by pressure variation. Figure 11 shows force variation as a wheel passes over a 3mm insulated joint at 125 kph, and shows the corresponding worn rail surface after 2, 4 and 6 MGT. (For a 20-tonne axle load, i.e., 100kN average normal contact force, 100000 wheel passes corresponds to 2 MGT.)

Note:

- For the predictions in Figure 11, the average wear rate equation is used for the first 100000 cycles, and the asymptotic wear rate equation is used subsequently.
- Traction coefficient t_c=0.1 has been chosen (with friction coefficient μ=0.45), appropriate for distributed traction vehicles.
- The gaps in the curves are regions where the contact patch ellipticity differs significantly from 1.32.

Both wear rate equations are linear functions of pressure (which is proportional to the cube root of the normal force), for a fixed traction coefficient, so the final wear pattern will be a linear function of pressure.

3.4.1 Summary and conclusions:

Wear rate equations developed in D4.2.5 have been used to predict rail surface change through wear. For a fixed traction coefficient, the final wear pattern is a linear function of pressure, which is in turn proportional to the cube-root of the applied normal force. The highest wear is immediately after the insulated joint, with additional high-wear spots appearing a few metres later as the wheel bounces down and settles.

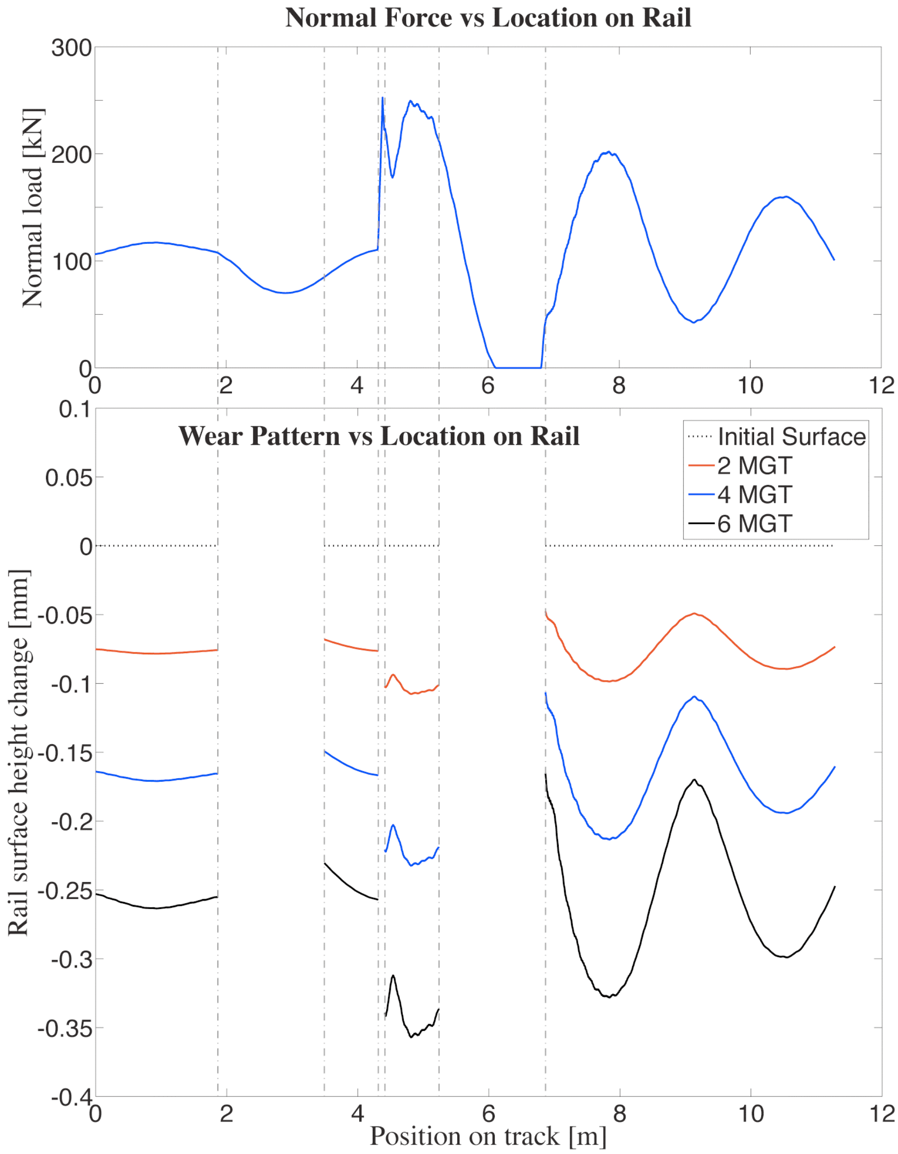

Figure 11 *Top: Wheel-rail contact force variation as a wheel passes over a 3mm insulated joint at 125 kph (adopted from Kabo et al., 2006). Bottom: Corresponding wear pattern (worn rail surface) after 2, 4, and 6 MGT. Traction coefficient is 0.1. The gaps are regions where the contact patch ellipticity differs significantly from the 'standard' 1.32.*

4. Concluding remarks

Numerical simulations have been carried out to assess the influence of key parameters on the deterioration of insulated joints. Simulations of plastic deformation show that the rail head edge at the insulation is severely strained. The accumulated plastic strain after four load passages, ε_{eff}, was adopted to quantify the ratcheting strain. The numerical simulations showed that increasing the insulating gap from 4 mm to 6 mm gives roughly the same effect as an increase of the vertical load from 150 kN to 200 kN. In addition, a very detrimental effect of traction and braking was found: Increasing the longitudinal load from 0 kN up to 45 kN caused an increase in ε_{eff}, magnitudes with up to 95%.

The predictions of plastic deformation and rolling contact fatigue have been performed. A fixed traction coefficient was presumed giving a wear pattern that is a linear function of pressure, which is in turn proportional to the cube-root of the applied normal force. The highest wear is predicted immediately after the insulated joint, with additional high-wear spots appearing a few metres later as the wheel bounces down and settles.

In addition to numerical simulations, four operational joints have been monitored to follow the degradation. It was found that material damage is induced very fast. In accordance to numerical simulations the rail ends closest to a nearby station showed the largest degree of (wear like) damage. After 8 months it was found that also “cavity-like” damages had formed in the vicinity of the insulating joint.

The studies will continue in two forms during the spring of 2009:

- A Master of Science project will be devoted to continued numerical simulations of joint degradation and investigation of possible relieving actions.
- The field studies will continue to gather more understanding of the operational mechanisms.

The conclusions from these studies along with operational guidelines will be presented in the upcoming deliverable report D4.2.6.

5. References

Y.-C. Chen and L.-W. Chen. Effects of insulated rail joint on the wheel/rail contact stresses under the condition of partial slip. Wear, 260:1267–1273, September 2006.

Y.-C. Chen and J. H. Kuang. Contact stress variations near the insulated rail joints. Proc Inst Mech Eng Part F J Rail Rapid Transit, 216:265–274, 2002.

A. K. Himebaugha, R. H. Plaut, and D. A. Dillard. Finite element analysis of bonded insulated rail joints. Int J of Adhesion and Adhesives, 28(3):142–150, April 2008.

Y. Jiang and H. Sehitoglu. A model for rolling contact failure. Wear, 224:38–49, Jan 1999.

G. Johansson. On the modeling of large ratcheting strains and anisotropy in pearlitic steel. PhD thesis, Chalmers University of Technology, Department of Applied Mechanics, Chalmers SE 412 96 Göteborg, Sweden, 2006.

G. Johansson and M. Ekh. On the modeling of large ratcheting strains with large time increments. Engineering Computations, 24:221–236, 2007.

G. Johansson and M. Ekh. On the modeling of evolving anisotropy and large strains in pearlitic steel. European Journal of Mechanics, A/Solids, 25:1041–1060, November/December 2006.

G. Johansson, M. Ekh, and K. Runesson. Computational modeling of inelastic large ratcheting strains. International Journal of Plasticity, 21:955–980, May 2005.

G. Johansson, J. Ahlstrom, and M. Ekh. Parameter identification and modeling of large ratcheting strains in carbon steel. Computers and Structures, 84:1002–1011, June 2006.

E. Kabo. Förstudie. isolerskarvars inverkan på spårets mekaniska egenskaper: en finit elementanalys. Research report 2004:14, Chalmers University of Technology, Department of Applied Mechanics, Chalmers SE 412 96 Göteborg, Sweden, 2004 (In Swedish).

E. Kabo, J. C. O. Nielsen, and A. Ekberg. Prediction of dynamic train-track interaction and subsequent material deterioration in the presence of insulated rail joints. Vehicle System Dynamics, 44:718–729, 2006.

R. H. Plaut, H. Lohse-Busch, A. Eckstein, S. Lambrecht, and D. A. Dillard. Analysis of tapered, adhesively bonded, insulated rail joints. Proc Inst Mech Eng Part F J Rail Rapid Transit, 224:195–204, 2007.

J. Sandström. Analysis of rail breaks and insulated joint deterioration. LicEng thesis, Chalmers University of Technology, Department of Applied Mechanics, Chalmers SE 412 96 Göteborg, Sweden, 2008.

J. Sandström, A. Ekberg, and E. Kabo. Isolerskarvar — jämförelse mellan 4 mm och 8 mm skarvöppning. Research report, Chalmers University of Technology, Department of Applied Mechanics, Chalmers SE 412 96 Göteborg, Sweden, 2006. In Swedish.

D. Socie and G. B. Marquis. Multiaxial Fatigue. SAE International, Warrendale, PA USA, 2000. ISBN 0768004535.

UIC. Leaflet 712R Rail defects. Paris, France, fourth edition, Januari 2002. ISBN 2-7461-0341-9.

6. Annexes

I Johan Sandström & Anders Ekberg, A numerical study of the mechanical deterioration of insulated rail joints, IMechE Journal of Rail and Rapid Transit (in press)